ACS APPLIED MATERIALS & INTERFACES

Research Article

www.acsami.org

Structural Iridescent Tuned Colors from Self-Assembled Polymer Opal Surfaces

Laura Zulian,*[,†] Elisa Emilitri,*[,†] Guido Scavia,[†] Chiara Botta,[†] Miriam Colombo,[‡] and Silvia Destri[†]

[†]Istituto per lo Studio delle Macromolecole, CNR-ISMAC, Via Bassini 15, 20133 Milano, Italy

[‡]University of Milano-Bicocca, Piazza della Scienza 2, 20126 Milano, Italy

Supporting Information

ABSTRACT: Structural colors are the object of a wide scientific interest, not only for the potential technical applications of their intriguing optical properties but also for the need of coloring agents to replace toxic and carcinogenic dyes. We present a simple methodology to obtain polymer opal surfaces of self-assembled core–shell nanoparticles with different degree of order for structural color applications. Polymer nanospheres prepared by surfactant-free emulsion radical copolymerization of an hydrophobic and an hydrophilic comonomer (styrene and methacrylic acid) spontaneously assemble into core–shell particles. Nanoparticles with identical composition and different diameters were prepared by modulating the degree of ionization of the weakly acidic comonomer. We report experimental results revealing how the synthesis parameters affect the properties of the core–shell particles and their influence on the optical properties of the final polymer opal surfaces, which depend on size, charge, and packing arrangement of the constituent nanoparticles.

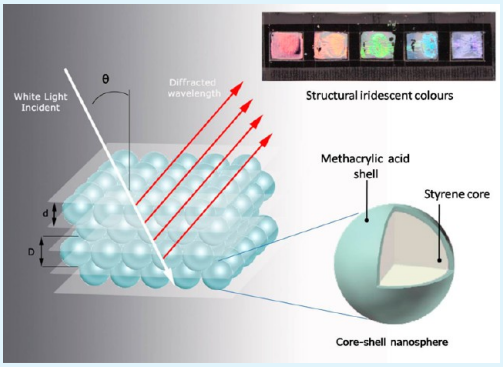

KEYWORDS: *colloidal crystals, structural color, diffraction, nanoparticles, self-assembly, surfactant-free emulsion polymerization*

INTRODUCTION

Periodically textured materials are often used by nature to create brilliant colors of purely physical origin, because of the diffraction or interference of multiple light paths. Significant examples of such complex architectures are found in the colorful world of insects,[1,2] butterflies,[3−5] birds[6,7] and minerals[8,9] in which many hues and optical effects are the results of structural colors. Structural coloration is not subject to photobleaching and it can also create color effects not achievable merely through pigments. Scientists are exploiting these mechanisms to produce tunable colored surfaces for a wide variety of optical[2,3,10−13] and technological applications[14−16] or simply as coloring agents to replace toxic and carcinogenic dyes.[16−18] The complex architectures underlying such optical properties are called *natural photonic crystals*, ordered dielectric composite structures with periodicities ranging from a few hundred nanometers to several micrometers. These structures affect the light propagation with wavelength comparable to the variation-periodicity of the photonic crystal due to Bragg diffraction events. When these wavelengths are within the visible range, brilliant and iridescent colour effects can be observed. One of the most promising and inexpensive ways to fabricate ordered architectures at visible wavelengths is the use of colloidal particles.[19] Among these, particles with a core–shell structure have recently aroused special interest. Previous studies focused, for example, on the tuning of the core–shell ratio to control the position and the width of the wavelength stopgap,[20] or on the incorporation of particles of different size into the interstices of core–shell particles crystals in order to modify the final color of the surface.[17] Moreover, the effect of refractive index contrast modification in the interparticle medium,[21] the engineering of the chemical core–interlayer–shell precursor particles composition,[22] or the fabrication of full color colloidal crystals with a tough mechanical strength[18] have been investigated. The preparation process presented in this paper is a simple, industrially scalable approach to produce polymeric opal surfaces of self-assembled core–shell nanoparticles for structural color applications based on surfactant-free emulsion polymerization (SFEP). SFEP is one of the most interesting techniques emerged in recent years to prepare polymeric monodisperse or quasi-monodisperse nanoparticles in the micrometer and submicrometer range,[23] which makes them especially suitable for the preparation of photonic crystals with synthetic opal structure. The intrinsic simplicity and efficiency of this technique make it a very attractive option when large-scale and repeated batch production is desired. Many different SFEP procedures have been reported,[24] mostly involving polystyrene and methacrylic monomers as the dispersed hydrophobic phase. Special interest has been shown in the case of the SFEP preparation of copolymers of two or more monomers with a marked difference in hydrophilic properties, which leads to the synthesis of monodisperse core–shell particles in a single step. In this case, the hydrophobic

Received: August 19, 2012
Accepted: October 11, 2012
Published: October 11, 2012

   dx.doi.org/10.1021/am301709b | *ACS Appl. Mater. Interfaces* 2012, 4, 6071−6079

monomer (usually styrene) ends up in the core, while the hydrophilic groups (often acrylic acid) create a soft, hydrated shell with exposed functional groups and ionic charge. The complete micelle formation and polymerization mechanism of SFEP is still not completely clear, especially in its earliest stages, even if some mechanisms have been proposed[23] for homopolymer micelle synthesis. In this work, we study the behavior of a simple model system obtained by SFEP of styrene (STY) and methacrylic acid (MA). Control over the resulting micelle size is achieved by changing the monomer ratio and the degree of hydrophilic monomer ionization. We are thus able to create several types of solid monodisperse copolymer micelles with a rigid polystyrene core and a soft hydrated corona of MA, that can self-assemble into solid-state patterns with different degrees of order, creating many structural colors. The properties of these self-assembled surfaces are studied in order to correlate nanoparticles structure and polymerization conditions to different optical reflectance spectra.

The objective of this work is to investigate how the synthesis parameters affect the final characteristic of the core−shell particles produced by SFEP. The effect of the synthesis pH and the weight percentage ratio (R) of methacrylic acid to the total amount of monomers (STY + MA) on the size of the core−shell particles is discussed. A series of polymer opals surfaces are created from the colloidal dispersion of different core−shell particles by casting. Finally, a deep investigation of their optical properties is carried out and discussed as a function of dimensions, charge, and packing arrangement of the constituent core−shell nanoparticles.

EXPERIMENT AND CHARACTERIZATION

Materials and Methods. All chemicals are purchased from Sigma−Aldrich and used without further purification, except styrene (STY). STY is washed with a 1 M KOH solution to eliminate the stabilizer (4-*tert*-butyl catechol) and then with water until neutrality. Doubly distilled water is used in the synthesis, while Milli-Q water (Millipore, Bedford, MA) is used in the purification and characterization steps.

Synthesis Procedure. Core−shell nanoparticles are prepared as reported in the literature[25,26] by surfactant-free emulsion radical polymerization at 100 °C under stirring. With R being the weight percentage ratio of methacrylic acid (MA) to the total amount of monomers (STY + MA) (R = wt MA/(wt MA + wt STY)), samples are prepared keeping constant the ratio between styrene and water (3:10 = styrene:water) and varying R. For each monomer ratio R, a series of syntheses is performed; in each preparation batch, the pH of the reaction medium is increased, adding different quantities of NaOH, in order to obtain samples with a different neutralization degree of MA. Here, the procedure details for the sample with R = 3.58 and pH 4.06 are given as an example. In a two-necked flask equipped with a condenser, magnetic stirring, and a heating bath, 6 mL (5.454 g, 0.524 mol) of styrene are mixed with 0.2 mL (0.203 g, 2.358 mmol) of methacrylic acid (MA) and suspended in an aqueous solution (20 mL of water) under vigorous stirring. Sodium hydroxide (18.8 mg, 0.47 mmol, 20% mol/mol of MA) is added to create the internal buffer and the mixture is heated under reflux for 10 min before adding the initiator. Potassium persulfate (25 mg) is then added and the polymerization is still allowed to proceed at reflux for 90 min. The resulting white latex is purified by tangential flow filtration, using Milli-Q water in a Millipore Pellicon XL Biomax 1000 cassette with a nominal cutoff of 1 million. Samples are dried and redissolved in appropriate solvents for SEC and NMR characterizations, while films are drop-cast on clean glass slides for AFM and optical measurements. About 50 mg of the dried material are dissolved in chloroform and cast as a thin film for Fourier transform infrared (FTIR) spectroscopy.

Film Casting. A glass slide is accurately cleansed by washing with detergent, followed by abundant washing with deionized (DI) water and finally dried under nitrogen flux, and a silicone rubber ring is applied on it to create a mold. Some drops of the purified nanoparticle dispersion (∼500 μL) are used to fill the mold. The drop spreads over the accessible glass surface contained by the ring. The quantity of the aqueous dispersion poured into the silicon container is enough to obtain a final thickness of some micrometers. The liquid is left to evaporate at room pressure and temperature to allow the formation of a thin vivid iridescent colloidal crystal.

Characterization. Polymer nanoparticles are characterized by size exclusion chromatography (SEC), nuclear magnetic resonance (NMR), zeta potential, static light scattering (SLS), dynamic light scattering (DLS), atomic force microscopy (AFM), and transmission electron microscopy (TEM) measurements. SEC is performed with tetrahydrofuran (THF) as the mobile phase, using an integrated Alliance 2695 chromatographic system, calibrated toward polystyrene, from Waters (Milford, MA) and a 2414 differential refractometer detector (DRI). NMR spectra are recorded using a Bruker Advance 400 spectrometer in deuterated chloroform ($CDCl_3$) and THF-d_8. FTIR of polymer thin films are recorded using a Bruker Tensor 27 spectrometer and elaborated using OPUS software. High-resolution transmission electron microscopy (HRTEM) measurements are performed with a Zeiss HRTEM LIBRA200 system on samples obtained by casting a drop of solution onto a carbon-coated grid. A 1 M phosphate buffer at pH 7.4 solution is used for SLS, while DLS and zeta potential are measured in diluted Milli-Q water solutions. SLS is performed using a DAWN Wyatt multiangle light scattering instrument equipped with an He−Ne laser (λ = 632.8 nm) light source. The scattered intensity is recorded simultaneously by 18 discrete photo detectors over a broad range of scattering angle θ (from 4° to 160°). Each analogic signal is processed and the data collected using the ASTRA software. From these data, the gyration diameter (D_g) of the core−shell particles can be measured. Hydrodynamic diameter, polydispersity, and zeta potential of the core−shell nanoparticles are determined using a Brookhaven 90 Plus size analyzer. The apparatus is equipped with an He−Ne laser emitting light at λ = 632.8 nm and a detector recording intensity at a fixed scattering angle θ = 90° . The hydrodynamic diameters are measured at room temperature. For further details about these experimental techniques, see the Supporting Information (SI) material. Zeta potential measurements are recorded on the same instrument using an AQ-809 electrode. Data are processed by Zeta Plus Software.

The morphology of the polymer opal surfaces and their different aggregation behavior are studied by AFM, using a NT-MDT NTEGRA instrument in noncontact and tapping mode under ambient conditions. Grain analysis is performed with NT-MDT grain analysis software where the mean length of each particle corresponds to the diameter of the equivalent sphere. The thick samples are not transparent to the visible radiation, thus optical diffraction experiment are performed in a reflection mode. Our setup consists of a xenon lamp coupled with a double grating monochromator in order to investigate

the entire range of visible wavelengths (400−700 nm). The light beam exiting the monochromator passes through a chopper and it is collimated by a lens before reaching the sample which is mounted vertically on a horizontal rotating stage. A Si photodiode mounted on a rotating arm detects the reflected light at any angle. The signal is acquired by a lock-in amplifier and processed through a self-developed Labview software.

RESULTS AND DISCUSSION

SFE copolymerization to form core−shell micelles has attracted huge interest, because of its simplicity and reliability. However, the dependence of the system behavior on several parameters, makes it particularly challenging to control. In this paper, a simple and efficient model system based on styrene (STY) and methacrylic acid (MA) is investigated. While the effect of comonomer solubility and initiator concentration has already been studied for similar systems,[23,27] we mainly focus on the effect of copolymer composition varying the monomers ratio and the neutralization degree of the acidic comonomer.

Three series with different acid contents are prepared (namely, R = 3.24%, R = 3.58%, and R = 4.10%). An increasing quantity of NaOH from 0 to 75% is added in order to obtain different internal buffer pHs, as reported in Table 1. Over this limit, the monomer dispersion is not stable and it collapses. Reaction medium pH is calculated for each sample; since the internal buffer is formed before adding the polymerization initiator, the pK_a value for MA (pK_a = 4.66) is used as a valid value for calculation. After the polymerization the micelle structure obtained with each set of parameters is stable and does not rearrange if the particles are suspended in new medium at different pH. A summary of the prepared samples is reported in Table 1, as a function of composition R and the pH of the synthesis medium. Varying the R and pH parameters, we are able to modify the characteristic radius of the particles and their surface charge acting on the deprotonation of the carboxyl groups of the MA. We will show that, by varying these parameters, we are able to obtain a fine-tuning of the core−shell nanoparticles size and the modification of the long-range interactions among them during the formation of the colloidal solid phase, resulting in quite different final optical properties. We start our characterization by the study of the single polymer chains. SEC, FTIR, and NMR are used to study composition and molecular weight of the constituent copolymers by dissolving the structures in the appropriate solvents (THF, $CHCl_3$, and THF-d_8, respectively) and casting them in a thin film for FTIR. From the NMR, we are able to confirm the completeness of the reaction due to the absence of detectable residual double bonds. Moreover, FTIR detects the presence of C═O groups in the copolymers while SEC chromatograms show the formation of high-molecular-weight polymer chains (M_w in the 500−2000 kDa range) with broad monomodal distribution, as expected in an emulsion polymerization (see the SI for details).

Table 1. Summary Table of the Samples Synthesized, Reporting the Methacrylic Acid (MA) Percentage, the Amount of NaOH Added, and the pH of the Resulting Buffer

R	NaOH (mol %)	reaction buffer pH
3.24% MA	0	2.88
	10	3.70
	20	4.11
	30	4.34
	50	4.74
	60	4.82
	75	5.22
3.58% MA	0	2.85
	4	3.33
	6	3.49
	8	3.56
	10	3.76
	20	4.06
	30	4.29
	50	4.66
	60	4.84
	65	4.93
4.10% MA	0	2.82
	20	4.06
	40	4.49
	60	4.84
	75	5.14

Particle Characterization and Effect of Synthesis pH. In order to characterize the synthesized particles obtained by the SFEP process described above, several experimental techniques are used. TEM images have been recorded in order to study particles shape and structure.

HRTEM analysis has been performed on particles dispersed onto the coated grid and, consequently, not still organized into a compact layer. The corresponding TEM images shown in Figure 1 refer to the case with R = 4.10% and pH 4.49 as an example. As shown in the figure, the particles are spherical and nearly monodisperse. The morphology of the system is expected to be a core−shell structure with an hydrophobic PS core and an hydrophilic MA shell. The hydrophilic shell is extremely thin, as expected, because of the very low MA content in the composition. Results describe an intermediate condition from solution to a solid "bulk" layer and show that an initial aggregation process already starts even when particles are relatively free (Figure 1c). This clusterization is favored by a

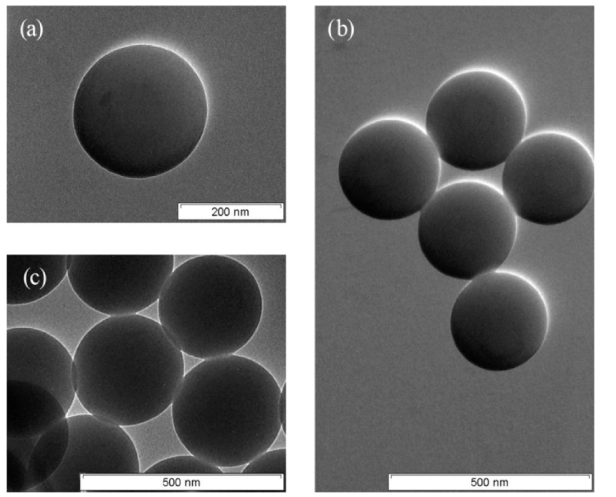

Figure 1. Three different TEM images referred to the R = 4.10% and pH 4.49 sample. (a) The particles are spherical and nearly monodispersed. (b,c) The fusion of the shells when two or more nanoparticles are in contact is evident.

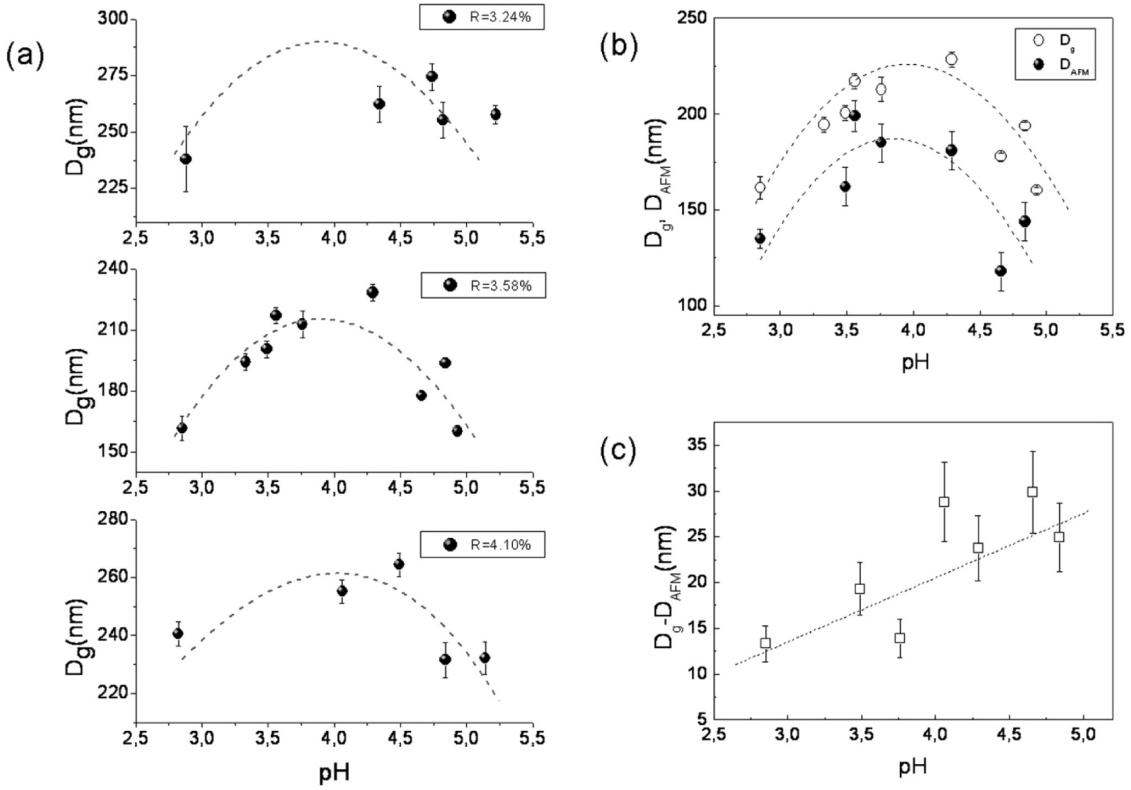

Figure 2. (a) Gyration diameter (D_g) of the core−shell nanoparticles in aqueous solution for different methacrylic acid (MA) contents R (top to bottom: R = 3.24%, R = 3.58%, and R = 4.10%) versus the pH of the synthesis medium. (b) Comparison between the gyration diameter in solution (D_g) and the diameter estimated by AFM measurements (D_{AFM}) of the core−shell particles with R = 3.58%. (c) Difference between D_g and D_{AFM} (estimated shell diameter) for the samples reported in panel (b). All dashed lines are in place only as guides to the eye.

fusion-like interaction between the hydrated shells as evidenced in Figure 1b. Finally, the diameter in this partially hydrated state (230 nm for this sample) of particles in Figure 1a is confirmed to be higher than the corresponding dry state (205 nm, as measured by AFM).

Dynamic light scattering (DLS) measurements are carried out in order to estimate the hydrodynamic diameter (D_h) and the polydispersity of the suspended nanospheres in aqueous dispersion. The results show a DLS polydispersity of <0.02, corresponding to a very narrow size distribution, an important prerequisite to obtain the formation of an ordered opal. Static light scattering (SLS) is used to estimate particle diameter in solution (gyration diameter, D_g) and AFM microscopy is used to determine dry particle diameters (D_{AFM}) and shape. Nanoparticle structure is then studied by comparing the SLS and AFM diameters. Since the quantity of the hydrophilic monomer is small, we can consider the AFM diameter as a good approximation of the core diameter of nanoparticles, while the gyration diameter can be regarded as an estimate of the whole (core + hydrated shell) structure in water. The difference between these two measurements gives us an estimate of the swollen radius of the shell. Results show that, even in water, the shell radius is always <20% of the core radius, demonstrating that we have a crew-cut micelle-type system with a dense core and a thin shell of swollen chains.

The gyration diameters of the nanoparticles are shown in Figure 2a for different compositions (R = 3.24%, R = 3.58%, and R = 4.10% from top to bottom) versus the pH of the synthesis medium. pH is an important parameter for synthesis control, because it changes the ratio between the methacrylic acid/methacrylate ion in the solution. This ratio is know to induce a structural change in the shape and size of crew-cut micelles obtained by self-assembly of prepolymerized diblock copolymers where the core−shell ratio due to the methacrylic acid/methacrylate ion ratio shows a nonmonotonic trend[29,30] caused by different shell swelling. In our case, starting from single monomer units instead of preformed copolymers and using buffered monomer dispersions, a very different trend is observed, as shown in Figure 2a for all the different series and, more clearly, in Figure 2b, for one series only (R = 3.58%). Figure 2b reports a comparison between the gyration diameter (D_g) in solution and the dry diameter estimated by AFM for the series with R = 3.58%. As shown by this figure, an increase in particle diameter mainly due to a rise in core dimensions is observed for low neutralization degrees (NaOH/MA ≤25% mol/mol). This suggests that, the presence of Na^+ ions in the partly neutralized outer shell increases the efficiency of MA as a surface active agent, allowing the stabilization of larger particles. However, a further increase in medium pH, when NaOH/MA is between 25% and 75% mol/mol , results in a sharp decrease in the diameter of both the hydrated and dry particles. This decrease may be either due to an excess in surface charge density, as described in ref 29, where a larger area is required to allow all the ionic groups to be exposed to the aqueous solution or to a faster nucleation mechanism, because of the higher water solubility of methacrylate monomers.[31] Finally, the thickness of the hydrated shell, shown in Figure 2c, increases monotonically as the degree of neutralization increases, because of a higher extent of chain stretching, as expected from the literature data.[29]

From a direct combination of SLS and DLS techniques, we can define the ratio between the mean-square gyration diameter

(D_g) and the hydrodynamic diameter (D_h) obtaining the dimensionless parameter

$$\rho = \frac{D_g}{D_h}$$

This parameter is a sensitive tool for monitoring the changes in the shape and density of the particles. This ratio is given as ρ = 0.77 for monodisperse hard spheres of constant density, ρ = 1 for vesicle structures, and ρ = 1.50−1.78 in the case of random polymer coils. All the investigated samples have ρ values that fall into the 0.77−1.00 range, indicating an intermediate structure between a hard sphere and a vesicle.[28] In conclusion, DLS, LS, TEM, and AFM measurements all indicate a core−shell structure, with a prevalence of the hydrophilic comonomer in the shell and most of the PS monomeric units inside the core.

Self-Assembly and Characterization of the Polymer Opal Surfaces. Approximately 500 μL of the core−shell nanoparticles dispersion in water (ca. 20 wt %) is drop-cast on a flat glass substrate. The volume of the drop is chosen to provide the formation of a densely packed solid-state film with a thickness of some micrometers after evaporation of water. Polymer colloidal particles are not thermodynamically driven to assembly into the lowest energy state, they need an input of energy or external/directional force to assist their self-organization: in our case, capillary forces, because of the confinement of the liquid, assist the colloidal self-assembly. During the drying process, the concentration in the sample increases due to the water evaporation and, as the liquid layer thins, the nanoparticles come closer and closer. Collisions happen due to Brownian motion and some ordered aggregation phenomena start on the surface of the liquid giving origin to brilliant color effects. Also, the appearance of Newton rings can be noticed where the layer is thinner. The growth of an ordered array usually starts in the middle of the glass substrate, where the layer becomes thinner earlier. The ordered zone is surrounded by a thicker and slightly concave meniscus region in which nanoparticles are still free to move and are incorporated into the growing ordered phase upon reaching its boundary. After the complete evaporation of water, a polymer opalescent surface is formed whose specific optical properties are dependent on many parameters. A deep characterization of the polymer opal is performed using optical measurements and AFM. From the AFM images of the surfaces, we can obtain information on the shape, the diameter, and the arrangement of the nanoparticles after the drying process, while the reflectance spectra allow us to connect the optical properties of the surface with the structural properties of the solid phase. Each opal-like sample obtained by self-assembly of the core−shell nanoparticles shows an intense and brilliant coloration when exposed to white light.

In Figure 3, a schematic representation of the typical behavior of an opal structure is shown. The idealized structure of the colloidal crystal is presented in Figure 3a. Nanoparticles with diameter D are organized on parallel crystal planes, where d_{111} is the spacing between adjacent lattice planes. Each nanoparticle has a core−shell structure as shown in Figure 3b constituted by a rigid core of styrene and a shell of methacrylic acid (MA). When white light hits the surface with a incident angle θ on a such structure, only a certain range of wavelengths will be diffracted, depending on structural characteristic. This causes the crystal surface to appear with different colors ranging

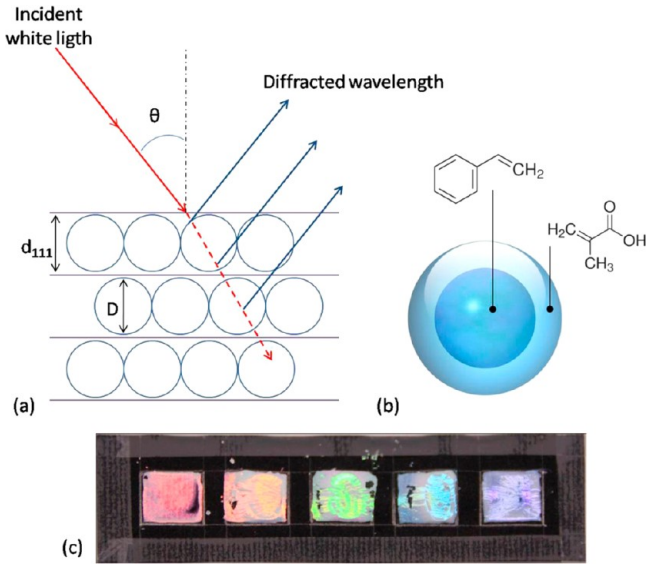

Figure 3. (a) Schematic representation of the optical behavior of an ideal colloidal opal. (b) Colloidal crystals are obtained by self-assembly of micelle-like polymer nanoparticles with a core of polystyrene and a shell of methacrylic acid (MA). (c) When a white light hits these structures, only a certain range of wavelengths will be diffracted, and different colors will be observed on the surface (from left to right, the sample preparation parameters are as follows: pH 4.49, R = 4.10%; pH 4.06, R = 4.10%; pH 2.88, R = 3.24%; pH 4.93, R = 3.58%; pH 2.85, R = 3.58%).

in the entire visible spectrum from red to blue. In Figure 3c, a photo of five different colloidal crystal samples is reported, corresponding to core−shell particles with dry diameters of D_{AFM} = 221, 209, 187, 144, and 135 nm, from left to right. We have performed an optical characterization of the colloidal surfaces through the analysis of the Bragg reflection spectrum of each sample. A narrow optical reflection band is observed for each sample attesting the regularity of the self-assembled opal surfaces. This is another proof of the narrow size distribution of the nanoparticles, because only colloids with a narrow size distribution are able to crystallize into opal structures. The optical properties of a crystalline lattice, specifically the Bragg reflection peaks, are dependent on several parameters, one of the most important being the dielectric contrast, which controls the spatial modulation percentage of the dielectric constant. When a colloidal crystal is composed of two spatially alternating materials a and b, the contrast parameter is dependent on the dielectric constants of the two materials (ε_a and ε_b). For an opal-like system, ε_a is the dielectric constant of the spherical particles, while ε_b is the dielectric constant of the interparticles matrix. In our case, the space between adjacent particles is occupied by air; then, we assume ε_b = 1. From the measurements of the Bragg reflection spectra, we can obtain reliable information on the geometrical and morphological parameters of the crystals.

The optical reflectance spectra of a typical sample are reported in Figure 4a. The Bragg reflection spectra are recorded by varying the light incidence angle θ from 6° to 46°, counted from the normal to the sample plane. As the angle θ becomes larger, the reflection peaks are shifted toward shorter wavelengths. The positions of the Bragg reflex peaks are shown in Figure 4b, as a function of the light incidence angle. This angular dependence is well-described by Bragg's formula:

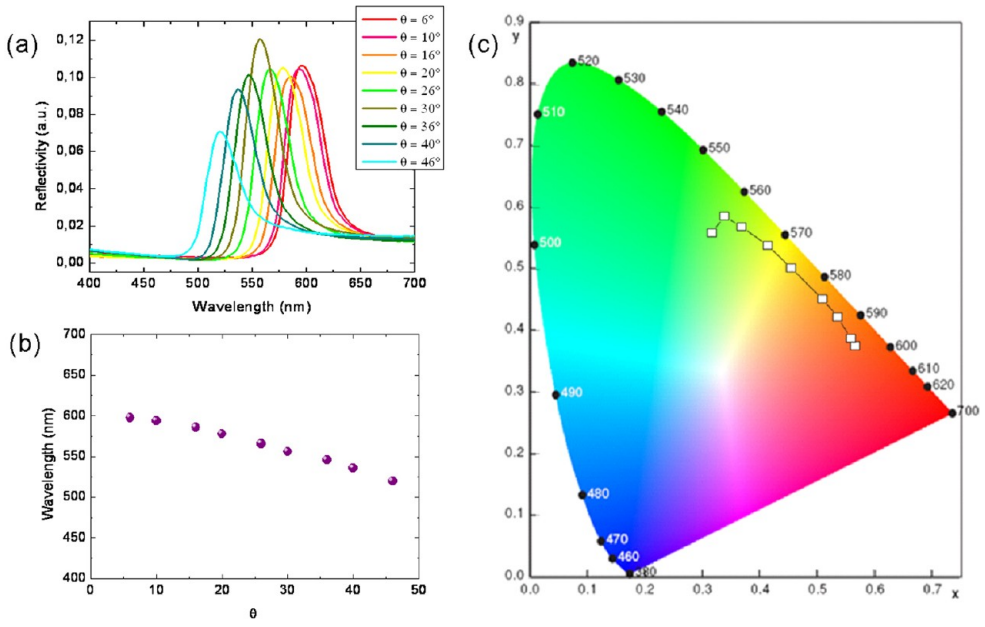

Figure 4. (a) Optical reflectance spectra recorded at various incident light angles are reported for a sample with R = 3.24% and synthesis medium pH 4.34. (b) The positions of the Bragg maxima, as functions of θ, are indicated as points. (c) The perceived color iridescence curve of the sample, as reported on a CIE xy chromaticity diagram.

$$\lambda = 2d_{111}\sqrt{\varepsilon_0 - \sin^2\theta} \quad (1)$$

where λ is the wavelength at the reflection peak, d_{111} the spacing between adjacent lattice planes, θ the incidence angle, and ε_0 the average dielectric constant of the composites:

$$\varepsilon_0 = \varepsilon_a f_0 + \varepsilon_b(1 - f_0) \quad (2)$$

where f_0 is the filling fraction for the structure. It should be noticed that the filling fraction f_0 can vary among samples and it can influence the characteristic structural color obtained in the final film as strongly as the dimension of the spheres. The iridescence effect of the sample was reported on a CIE xy chromaticity diagram, in order to give a more direct idea of the color hues range exhibited by the opal surface (Figure 4c). One of the most important parameters that controls the final coloration of the surface is the size of the particles composing the solid phase.[18,32]

Figure 5 displays the variation of the Bragg maxima of the spectra (measured with a light incident angle of 20° to the normal surface), as a function of the sphere size D_{AFM} obtained by AFM measurements. The peak position is red-shifted as the size of the spheres increases according to a linear relationship coming from the Bragg relation (eq 1). By varying the dimension of the core−shell particles, we are able to obtain any color in the visible range. The dashed line reported in Figure 5 represents the ideal case of a close packed crystalline surface (either face-centered or hexagonal) constituted by spheres with a refractive index of n = 1.59 (polystyrene). In such a case, the particle diameter can be related to the lattice parameter d_{111} by the geometrical relation $d_{111} = (^2/_3D)^{1/2}$. Most of the experimental points deviate from the ideal behavior. In particular, we can also stress that surfaces constituted by particles with the same diameter D_{AFM} can show very different values for the Bragg reflectance peak, resulting in different coloration. This behavior can be explained considering another significant parameter which plays an incisive role in the determination of the final optical properties of the sample: the

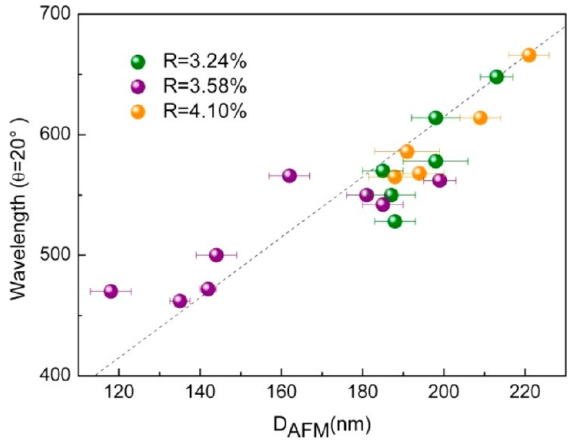

Figure 5. Position of the Bragg maxima (at a fixed incident light angle of θ = 20°), as a function of the dimensions of the dry nanoparticles measured by AFM. Colors reflect sample composition: green dots, R = 3.24%; purple dots, R = 3.58% ; orange dots, R = 4.10%). The dotted line shows the ideal trend from the Bragg equation, eq 1, assuming a perfectly close-packed structure (see text).

filling fraction f_0. The parameters d_{111} and f_0 can be obtained from the slope and the intercept of the linear relation between λ^2 and $\sin^2\theta$ easily derived from eq 1. The dielectric constant of the core−shell particle ε_a is considered equal to that of the polystyrene core, neglecting the contribution of the shell because of its small volume. Therefore, the dielectric constants for air (ε_b = 1.00) and polystyrene (ε_a = 2.60) were assumed for the fit from eq 1.

The position of the Bragg peaks, as a function of the square sine of the light incidence angle and their linear fit, are reported in Figure 6 for the same sample shown in Figure 4. The linear fit well describes the angular dependence of the peak position, giving d_{111} = 205 nm and f_0 = 0.68. The resulting value of d_{111} is consistent with the diameter obtained from AFM measurements (D_{AFM} = 198 ± 5 nm) while the value of the parameter

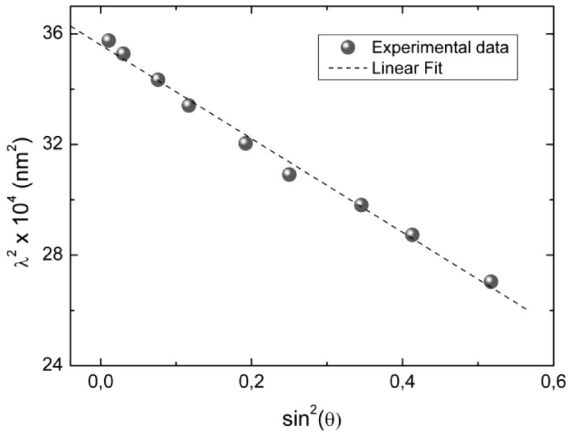

Figure 6. Angular dependence of the Bragg peaks for the sample with R = 3.24% and pH 4.34. The dashed line represent the linear fit of the experimental data (λ^2 vs $\sin^2\theta$) derived from eq 1.

f_0 indicates that the structure is not close-packed but similar to a random assembly of particles, whose f_0 value was estimated by Jaeger and Nagel to be 0.64.[33] As already noted, the effect of the packing arrangement must be taken into account in the determination of the final color of samples. To evaluate the effect of different packing arrangements, four samples with the same measured diameter in the solid state (mean diameter, D_{AFM} = 198 nm) are compared. Reflectance peaks recorded at the same angle of light incidence (θ = 20°) are reported in Figure 7, from top to bottom, for increasing values of the packing arrangement parameter f_0.

As highlighted from the dashed lines, the consequence of the increased value of f_0 is a shift of the Bragg maximum toward higher wavelengths. Next to each spectrum, the AFM image of the corresponding surface is shown, confirming the monodispersity of the core−shell particles and clearly showing that the increase of f_0 reflects the progressive extension of a close-packed order: the top panel has a value f_0 = 0.63, which is consistent with a totally random distribution of the core−shell spheres, while the bottom panel has a value of f_0 = 0.75, characteristic of a close-packed structure. Looking at the AFM images, from top to bottom, we can observe the growth of ordered domains and the progressive disappearance of the

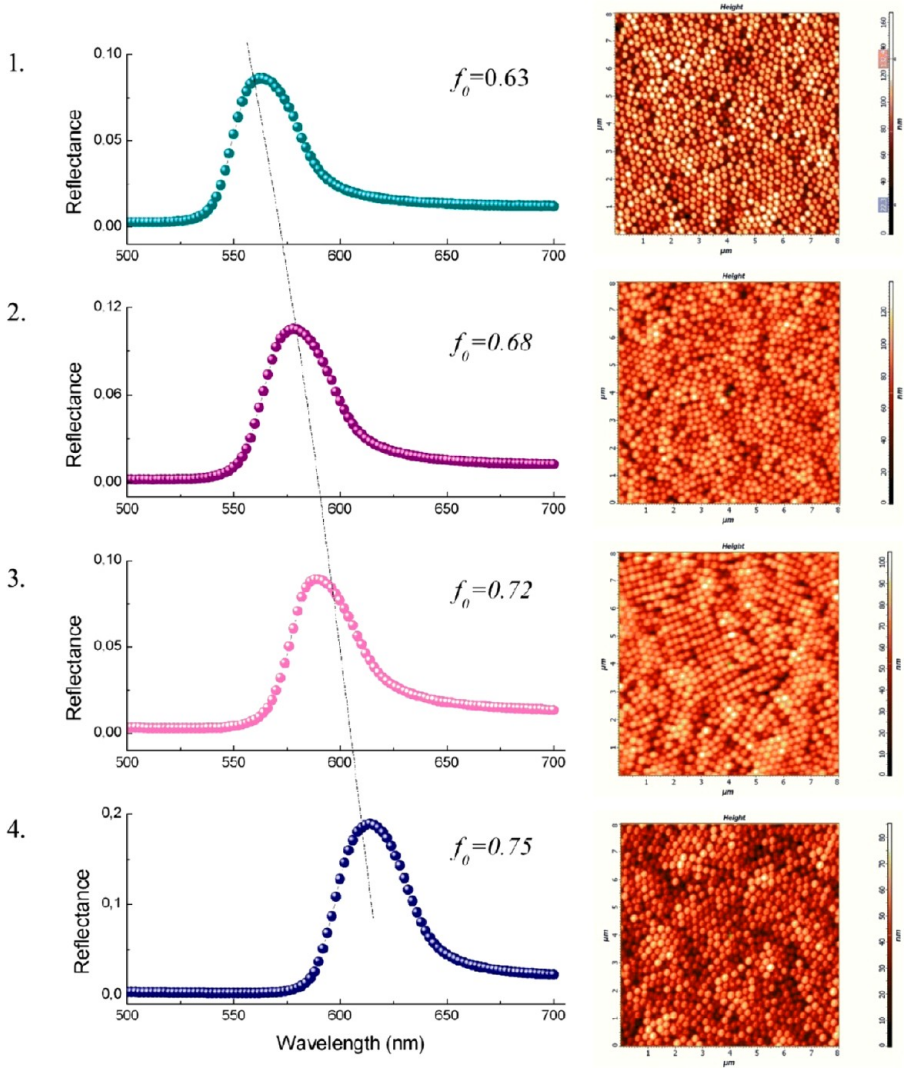

Figure 7. Effect of the packing arrangement on the Bragg peak's position for sample obtained from different nanoparticles with a mean dry diameter of D_{AFM} = 198 nm. Characteristic color is shifted toward red at increasing value of f_0. (From top to bottom, the synthesis parameters are as follows: pH 3.56, R = 3.58%; pH 4.34, R = 3.24%; pH 2.82, R = 4.10%; pH 4.06, R = 4.10%).

dx.doi.org/10.1021/am301709b | ACS Appl. Mater. Interfaces 2012, 4, 6071−6079

empty interparticle spaces. Therefore, surfaces obtained from core−shell particles with nominally identical dry diameter shift their characteristic final coloration toward red as the filling fraction grows and the structure approaches a perfect close packing. It is also worth to stress that different opal surfaces obtained by core−shell particles prepared under the same conditions show a reproducible optical behavior, indicating that the variation of the packing parameter observed in Figure 7 is not accidental but effectively due to a different aggregation behavior of the core−shell nanoparticles, independent of their size. A possible explanation of this phenomenon can be found in the surface charge of the nanospheres involved in the self-assembly process. The colloidal particles giving origin to the crystal surfaces shown in Figure 7 have been prepared using different synthesis parameters. Then, although the final diameter measured by AFM is the same for all the four samples, other intrinsic characteristics such as the radius of the hydrated corona and the surface charge, can be different. In order to further investigate the driving force involved in the particle self-organization, we have measured their zeta potential value. All of the samples are negatively charged, with high zeta potential values that account for the long-term stability of the nanoparticle latexes (up to months, even at relatively high particle concentration, e.g., 20 wt %). As discussed previously, all the particles have the same crew-cut micelle type of geometry, so the behavior of the acidic shell for the different samples should be analogous. As reported in Table 2, the zeta potential of the particles appears to be directly connected with their f_0 value in the solid state, with values increasing as f_0 increases.

Table 2. Summary Table of Characteristic Parameters Referred to Samples Reported in Figure 7

panel	D_{AFM}(nm)	f_0	zeta potential (mV)	wavelength peak (nm)
1	199 ± 4	0.63 ± 0.02	−36.85 ± 1.84	562 ± 3
2	198 ± 5	0.68 ± 0.03	−38.36 ± 1.53	578 ± 5
3	197 ± 4	0.72 ± 0.01	−48.68 ± 1.80	588 ± 3
4	200 ± 6	0.75 ± 0.03	−52.78 ± 2.63	614 ± 4

This observation agrees with literature findings on colloidal crystals formed from drop-cast suspensions and solvent evaporation, which are known to be more highly ordered, increasing particle surface charge.[34]

A linear dependence of zeta potential with methacrylic acid (MA) content was observed for the samples prepared from the free acid (that is without the presence of NaOH in the synthesis medium), as shown in Figure 8.

An increase in the MA percentage results in a larger zeta potential, probably because of a larger number of available acidic groups on the surface and within the shell. Therefore, for the range of compositions considered, the zeta potential is controlled only by the quantity of MA in the reaction mixture. Fixing this parameter, we can control the interparticle interactions due to electrostatic forces and then the order parameter f_0. As stated in the earlier paragraphs, within the same composition, we can use the quantity of added base in the internal buffer of the reaction medium to vary the particle solid diameter (that is, the core diameter) independently from the MA concentration. By controlling both the micelle composition and the pH of its synthesis medium, we then can master the particle size and the assembly mechanism, independently

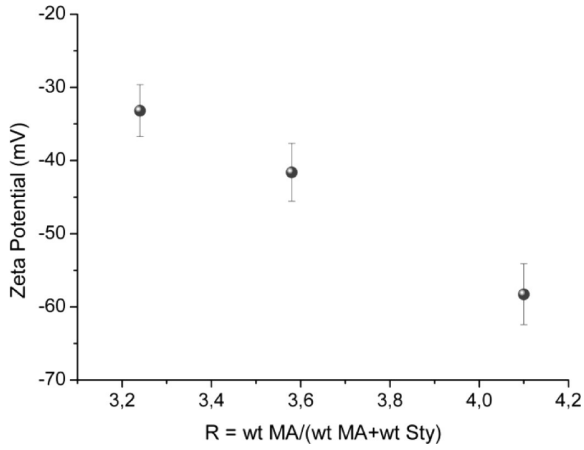

Figure 8. Zeta potential value as a function of the weight percentage ratio (R) of methacrylic acid (MA) for samples without added NaOH.

achieving separate control over both of the main parameters determining the optical properties of the final opal surface.

CONCLUSIONS

A simple methodology has been developed for the preparation of surfaces with defined iridescent optical properties. The proposed polymerization procedure allows to achieve control over the nanoparticle size and properties. A wide characterization of the core−shell particles both in solution and as self-assembled materials has been carried out in order to determine a relationship between the synthesis conditions and the final optical properties displayed by the surfaces. We found that the pH value and the methacrylic acid (MA) percentage (R) in the reaction medium influence both the size and the properties of the particles. The size of the core−shell particles is shown to be the most relevant parameter in the determination of the final optical properties of the film and, varying the parameters R and pH, core−shell particles can be synthesized with a size range wide enough to obtain the entire visible spectrum of colors. Another important result of this work is the observation that the final color of the dry surface is not dependent only on the size of the core−shell particles. We identify a new control parameter, the filling factor (f_0), which affects the organization of the spheres, causing particles with the same dry diameter to give origin to surfaces with different optical properties. At a fixed value of particle size an increasing value of f_0 provokes a shift of the Bragg maximum toward higher wavelengths. We show that f_0 is correlated to the intrinsic surface charge of the particles and it can be controlled by their chemical composition. In conclusion, we have developed a complete methodology to prepare iridescent surfaces using simple steps, and we show that, through the careful choice of a few synthetic parameters independently controlling both the particle dry diameters and their packing fraction, it is possible to finely tune the optical properties of the surfaces.

ASSOCIATED CONTENT

Supporting Information

This material is available free of charge via the Internet at http://pubs.acs.org.

AUTHOR INFORMATION

Corresponding Author

*E-mail addresses: laura.zulian@ismac.cnr.it, laura.zulian@gmail.com (L.Z.); elisa.emilitri@ismac.cnr.it (E.E.).

Notes

The authors declare no competing financial interest.

ACKNOWLEDGMENTS

This work was developed and founded within the GREEN COSMETIC project of Regione Lombardia.

REFERENCES

(1) Sharma, V.; MatijaCrne, M.; Park, J. O.; Srinivasarao, M. *Science* **2009**, *325*, 449−451.
(2) Deparis, O.; Rassart, M.; Vandenbem, C.; Welch, V.; Vigneron, J. P.; Lucas, S. *New J. Phys.* **2008**, *10*, 013032−013043.
(3) Huang, J. Y.; Wang, X. D.; Wang, Z. L. *Nano Lett.* **2006**, *6*, 2325−2331.
(4) Kinoshita, S.; Yoshioka, S.; Fujii, Y.; Okamoto, N. *Forma* **2002**, *17*, 103−121.
(5) Vukusic, P.; Sambles, J. R. *Nature* **2003**, *424*, 852−855.
(6) Blau, S. K. *Phys. Today* **2004**, *57*, 18−20.
(7) Vigneron, J. P.; Colomer, J. F.; Rassart, M.; Ingram, A. L.; Lousse, V. *Phys. Rev. E* **2006**, *73*, 021914−021921.
(8) Zakhidov, A. A.; Baughman, R. H.; Iqbal, Z.; Cui, C.; Khairulin, I.; Dantas, S. O.; Marti, J.; Ralchenko, V. G. *Science* **1998**, *282*, 897−901.
(9) Kavtreva, O. A.; Ankudinov, A. V.; Bazhenova, A. G.; Kumzerov, A. Y.; Limonov, M. F.; Samusev, K. B.; Sel'kin, A. V. *Phys. Solid State* **2007**, *49*, 708−714.
(10) Wang, J.; Zhang, Y.; Wang, S.; Song, Y.; Jiang, L. *Acc. Chem. Res.* **2011**, *44*, 405−415.
(11) Fudouzi, H.; Sawada, T. *Langmuir* **2006**, *22*, 1365−1368.
(12) Kim, S. H.; Lee, S. Y.; Yang, S. M.; Yi, G. R. *NPG Asia Mater.* **2011**, *3*, 25−33.
(13) Jorgensen, M. R.; Bartl, M. H. *J. Mater. Chem.* **2011**, *21*, 10583−10591.
(14) Fudouzi, H.; Xia, Y. *Adv. Mater.* **2003**, *15*, 892−896.
(15) Egen, M.; Braun, L.; Zentel, R.; Tannert, K.; Frees, P.; Reis, O.; Wulf, M. *Macromol. Mater. Eng.* **2004**, *289*, 158−163.
(16) Arsenault, A. C.; Puzzo, D. P.; Manners, I.; Ozin, G. A. *Nat. Photonics* **2007**, *1*, 468−472.
(17) Pursiainen, O. J. L.; Baumberg, J. J.; Winkler, H.; Viel, B.; Spahn, P.; Ruhl, T. *Opt. Express* **2007**, *15*, 9553−9561.
(18) Wang, J.; Wen, Y.; Ge, H.; Sun, Z.; Zheng, Y.; Song, Y.; Jiang, L. *Macromol. Chem. Phys.* **2006**, *207*, 596−604.
(19) Colvin, V. L. *MRS Bull.* **2001**, (August), 637−641.
(20) Velikov, P. K.; Moroz, A.; van Blaaderen, A. *Appl. Phys. Lett.* **2002**, *80*, 49−51.
(21) Gajiev, G. M.; Golubev, V. G.; Kurdyukov, D. A.; Medvedev, A. V.; Pevstsov, A. B.; Sel'kin, A. V.; Travnikov, V. V. *Phys. Rev. B* **2005**, *72*, 205115−205124.
(22) Spahn, P.; Finlayson, C. E.; MbiEtah, W.; Snoswell, D. R. E.; Baumberg, J. J.; Hellmann, G. P. *J. Mater. Chem.* **2011**, *21*, 8893−8897.
(23) Cheng, L. Z.; Han, C. C. *Macromolecules* **2012**, *45*, 3231−3239.
(24) Rao, J. P.; Geckeler, K. E. *Prog. Polym. Sci.* **2011**, *36*, 887−913.
(25) Gu, Z.-Z.; Chen, H.; Zhang, S.; Sung, L.; Xie, Z.; Ge, Y. *Colloids Surf. A* **2007**, *302*, 312−319.
(26) Reese, C. E.; Asher, S. A. *J. Colloid Interface Sci.* **2002**, *248*, 41−46.
(27) Wu, C. *Macromolecules* **1994**, *27*, 298−299.
(28) Schurtenberger, P.; Newman, M. E.; Buffle, J; van Leeuwen, H. P. In *Environmental Particles*, Vol. *2*; Lewis Publications: Boca Raton, FL, 1993.
(29) Zhulina, E. B.; Borisov, O. V. *Macromolecules* **2002**, *35*, 9191−9203.
(30) Matějíček, P.; Podhájecká, K.; Humpolíčková, J.; Uhlík, F.; Jelínek, K.; Limpouchová, Z.; Procházka, K. *Macromolecules* **2004**, *37*, 10141−10146.
(31) Preda, N.; Matei, E.; Enculescu, M.; Rusen, E.; Mocanu, A.; Marculescu, B.; Enculescu, I. *J. Polym. Res.* **2011**, *18*, 25−30.
(32) Subramania, G.; Constant, K.; Biswas, R.; Sigalas, M. M.; Ho, K.-M. *Appl. Phys. Lett.* **1999**, *74*, 3933.
(33) Jaeger, H. M.; Nagel, S. R. *Science* **1992**, *255*, 1523−1531.
(34) Li, F.; Josephson, D. P.; Stein, A. *Angew. Chem.* **2011**, *50*, 360−388.